Proceedings of the TMCE 2006, April 18–22, 2006, Ljubljana, Slovenia, Edited by Horváth and Duhovnik

PIECEWISE LINEAR CURVE RECONSTRUCTION FROM POINT CLOUDS

Oscar E. Ruiz
CAD/CAM/CAE Laboratory
Universidad EAFIT
oruiz@eafit.edu.co

Carlos A. Vanegas
CAD/CAM/CAE Laboratory
Universidad EAFIT
cvanega3@eafit.edu.co

ABSTRACT

Surface reconstruction from point samples must take into consideration the stochastic nature of the sample. This means, geometric algorithms reconstructing the surface should not insist in following in literal way each sampled point. Instead, they must interpret the sample as a "point cloud" and try to build the surface as passing for the best possible (in statistical sense) geometric loci that represents the sample. Two methods are presented in this paper, which respond to the stochastic nature of the sampling of a 1-manifold (a wire in 3-D). Both of them reduce the problem of quasi-planar samples to a problem in the XY plane. One of them uses the Voronoi Diagram and Delone Triangulation of the planarized sample to calculate the best possible tape-shaped polygon covering the point set, and then approaching the manifold with the medial axis of the polygon. The other method applies Principal Component Analysis to find a Piecewise Linear approximation of the same aforementioned medial Axis. Results are presented in the realm of Computer Vision applications. The authors seek to integrate the two methods in the near future.

KEYWORDS

Curve Reconstruction, Surface Reconstruction, Unorganized Points, Range Imaging, Principal Component Analysis, Least Squares Fitting, Delone Triangulation

1. INTRODUCTION

Reconstructing a curve or a surface from a point set is one of the most important problems in the reverse engineering of geometric models. In some cases curve reconstruction plays an important role in the surface reconstruction problem (Lee, 2000). It is the goal of this paper to present two methods involving statistical (Principal Component Analysis (PCA), Least Squares Fitting) and deterministic (Delone Triangulations) techniques for reconstructing a set of curves from clouds of unorganized points, and its application to surface reconstruction, using data sets resulting from optically capturing objects through range images.

This work will concentrate on planar or quasi-planar curves, since the statistical methods involved can be directly extended into $\mathbb{R}^3$. Two types of clouds of unorganized points have been considered. One of them consists in the clouds resulting from sampling and adding statistical noise to a set of C^1-continuous parametric curves $C_i(u)$ in $\mathbb{R}^3$. The point samples are supposed to comply with the Shannon or Nyquist criteria for digital sampling.

Problem Statement. Given a sample $S = \{P_0, P_1, \ldots, P_{N-1}, P_N\}$ from an (unknown) set of C^1-continuous (open or closed) parametric curves $C_i(u)$ in $\mathbb{R}^3$, a P.L. (Piecewise Linear) estimation of each $C_i(u)$ will be found.

The second type of clouds is related to range imaging. Range imaging offers an inexpensive and accurate means for digitizing the shape of three-dimensional objects. Because most objects self occlude, no single range image suffices to describe the entire object (Turk & Levoy, 1994), which makes necessary combining a collection of range images into a single polygonal mesh that completely describes the object. One of the steps of the proposed combination method, discussed in Section 5, involves generating several coplanar samples of points $S_1, S_2, \ldots, S_k, \ldots, S_K$, where $S_k = \{P_{0_k}, P_{1_k}, \ldots, P_{N-1_k}, P_{N_k}\}$, from the collection of shells recovered from the range images. The second type of clouds of unorganized points consists

in such clouds of coplanar sampled points (see Figure 2(a)).

In this case, we intend to find a P.L. estimation of the curve $C_i(u)$ that adequately fits the points in each of the clouds.

The mentioned types of planar or quasi-planar point samples are likely to include quasi-self-intersecting sections. For instance, in the case of a sample of an "8"-like section, two legal cross sections are equally likely: (a) two separate circular polygons, and (b) one polygon with thin waist. It is clear that near the self-intersecting point any algorithm may be confused. Another typical situation in surface reconstruction from planar samples is the one in which a particular level k is missing or incomplete (in the case of range imaging, this occurs when a portion of the object is not captured by any of the images). In such case, point samples from levels $k-1$ and $k+1$ are borrowed, and projected onto the insufficiently sampled plane. Naturally, the resulting cross section on plane k must then be recovered from a fuzzy point set. This point set should be treated with statistical tools, and the cross sections recovered should be the best fit to the planar point cloud contained in plane k.

Several solutions are available for curve reconstruction from organized point sets. However, the ordering of the points is unknown in most real problems. Several methods have been proposed for non-fuzzy sets. A survey on techniques for the case of closed, smooth, and uniformly sampled curves can be found in (Edelsbrunner, 1998). Methods for non-uniformly sampled smooth curves, and for uniformly sampled non-smooth curves are cited in (Althaus et al., 2000). Some TSP (Traveling Salesman Problem) and tour improvement heuristics were used by (Althaus & Mehlhorn, 2000), and good experimental results were reported. However, the reconstructed curve returned by these algorithms passes through each of the sampled points, and this type of solution is not adequate for the fuzzy point sets considered in this paper.

The methods proposed for the case of non-self-intersecting unorganized fuzzy sets include spring energy minimization (Fang & Gossard, 1992), implicit simplicial curves (Taubin & Ronfard, 1996), α-shape polygonal boundaries and medial axes (Edelsbrunner & Mücke, 1994), and moving least squares (Lee, 2000). A review of these methods along with their difficulties can be found in (Lee, 2000). A local search heuristic approach for self-intersecting unorganized fuzzy sets was used by (Verbeek et al., 2001) in a soft k-segments algorithm for principal curves. Good solutions were reported using this method. However, high values of k are required in order to return smooth P.L. approximations, and with the method involving local search algorithms, computational time might not be kept at reasonable levels.

Two methods for curve reconstruction that combine statistical and deterministic techniques are discussed in this paper. Section 2 examines the literature review of the statistical methods used. In Section 3 we discuss concepts necessary to implement the algorithms and their articulation in reaching the solution. Results for several types of point sets including non-smooth, self-intersecting, and non-uniform sets obtained with both methods are presented in Section 4. Section 5 describes an interesting integration of one of the methods to surface reconstruction from range images, and presents the results obtained for a real object. Finally, in Section 6 we draw the relevant conclusions, and propose bases for future work.

2. STATISTICAL APPROACH

The statistical approach for curve reconstruction from point samples had ancient precursors in Hastie and Stuetzle, 1989 (T & Stuetzle, 1989). In this reference, the authors define Principal Curves as smooth ones, which pass through the middle of, are self-consistent with, or are a principal curve of, a cloud of d-dimensional data sample with a probability distribution (μ, σ).

2.1. Principal Component Analysis

Although the following discussion treats point clouds in $\mathbb{R}^3$ and $\mathbb{R}^2$, for the reader may be useful to know that the stochastic analysis presented is applicable to samples in N dimensions (in fact, the Principal Component Analysis method was developed for treatment of samples in n-dimensional space, with $n >> 3$).

Given $S = \{p_i | p_i \in \mathbb{R}^n, 1 \leqslant i \leqslant m\}$ a set of m samples in $\mathbb{R}^n$. Without loss of generality one may assume that

$$\mu_1 = \mu_2 = ... = \mu_n = 0 \qquad (1)$$

meaning that the expected value of the n-dimensional distribution or the p_i's is the origin of $\mathbb{R}^n$. Let Σ be the covariance matrix of the m-size sample, where $\Sigma_{i,j}$ is the covariance of the i_{th} against the j_{th} component of the n-component p_i points.

One is interested in rotating S with a transformation R such that the new set $S' = \{q_i | q_i \in \mathbb{R}^n, 1 \leqslant i \leqslant m\}$ of transformed samples $q_i = R * p_i$ presents maximal dispersion in the direction of the first axis of $\mathbb{R}^n$, the second maximal dispersion in the direction of the second axis, and so on. For a point cloud that has a stochastic *linear* trend, establishing the direction of maximal dispersion is equivalent to identifying the direction vector of the line from which the sample was taken. For a point cloud with an stochastic *planar* trend, establishing the direction of minimal dispersion identifies the normal vector of the plane from which the sample was taken.

Let X_p, Y_p, Z_p unit vectors which note the directions in which S has the largest (σ_x), second largest (σ_y) and smallest variance (σ_z) respectively. It may be shown that

1. The pairs $(\pm X_p, \sigma_x)$, $(\pm Y_p, \sigma_y)$, and $(\pm Z_p, \sigma_z)$ are eigenvector - eigenvalue pairs of the Σ matrix.

$$\begin{aligned} \Sigma * (\pm X_p) &= (\pm X_p) * \sigma_x \\ \Sigma * (\pm Y_p) &= (\pm Y_p) * \sigma_y \\ \Sigma * (\pm Z_p) &= (\pm Z_p) * \sigma_z \end{aligned} \tag{2}$$

2. $\pm X_p, \pm Y_p, \pm Z_p$ are mutually orthogonal.

$$X_p \bullet Y_p = X_p \bullet Z_p = Z_p \bullet Y_p = 0 \tag{3}$$

3. $R * [X_p, Y_p, Z_p, O_p] = [X_w, Y_w, Z_w, O_w]$ and therefore:

$$R = \begin{bmatrix} X_p & Y_p & Z_p & O_p \\ 0 & 0 & 0 & 1 \end{bmatrix}^{-1} = \begin{bmatrix} X_p^T & 0 \\ Y_p^T & 0 \\ Z_p^T & 0 \\ O_p^T & 1 \end{bmatrix} \tag{4}$$

$[X_w, Y_w, Z_w, O_w]$ is the World Coordinate System or a fixed reference frame. Without loss of generality, one may assume that $X_w = [1,0,0]^T, Y_w = [0,1,0]^T, Z_w = [0,0,1]^T, O_w = [0,0,0]^T$ and therefore the right hand side of entry (3) above is a clipped 4×4 identity matrix. Equation (4) results from the completion of the identity matrix in entry (3) and its (trivial) inversion.

As a result, $[X_p, Y_p, Z_p O_p]$ is easily found and conforms a right handed coordinate system. In particular, $[X_p, Y_p, Z_p]$ is an orthonormal matrix. As desired, a parametric line $L(\eta) = O_p + \eta * X_p$ which crosses through the center of gravity of the point cloud S is found by sorting and naming the eigenvector-eigenvalue pairs such that $\sigma_x \geq \sigma_y \geq \sigma_z$.

Because of facts (2) and (4) it is clear that for quasi-planar data, the eigenvector Z_p associated to σ_z is the estimation of the direction normal to the plane, since σ_z is by definition the direction of minimal dispersion of the (planar) points. In converse way, for line data, the estimation of the direction vector of the line is the eigenvector X_p, since it is associated to the σ_x eigenvalue representing the maximal dispersion.

2.2. Least Squares Fitting

Section 2.1 illustrated how the coordinate system $[X_p, Y_p, Z_p, O_p]$ is calculated using PCA, by computing the eigenvector-eigenvalue pairs $(\pm X_p, \sigma_x)$, $(\pm Y_p, \sigma_y)$, and $(\pm Z_p, \sigma_z)$, of the Σ matrix. Because geometric kernels do not usually have available routines for calculation of n-dimension eigenpairs, a method was devised for the 3-dimensional case at hand. The method takes advantage of the fact that point samples from Coordinate Measurement Machines, Machine Tool stylos, CAT scans, etc., are planar or quasi-planar. As a consequence, a very close estimation of the lowest dispersion direction (the plane normal vector, Z_p) is easily achieved. The point cloud projected on this plane loses one dimension and therefore the problem becomes a 2-dimensional one. A solution of the eigenpair problem in Equation (2) can then be achieved as an extension of a Least Squares fitting. The LS method cannot be directly applied since it is dependent on the *implicit* form $y = mx + b$, which has no solution if m is the tangent of $\pm 90^o$. A random rotation, LS fitting and the corresponding counter rotation of the point data set avoids this problem and allows us to express the 3-D trend of the point cloud in terms of a *parametric* equation $L(\eta) = O_p + \eta * X_p$ which has no such indefinition.

In 2 dimensions, the Least Squares Method detects the trend m of a linear process. Since the 3-dimensional problem at hand is projected into 2-dimensional space, finding m in 2-dimensions is equivalent to calculating the projection of the direction vector X_p of $L(\eta)$ onto a plane. Because our point sample is quasi-planar only because of (machine tool) sampling errors, such a projection may be assumed *to be* X_p.

2.3. Point Sample Partition

Regardless of the method employed to estimate a PL approximation for the curves, it is capital to recognize

the fact that the data set must be partitioned into the data sets originated from the individual curves. For such a partition let us define an equivalence relation on the S point set:

An equivalence relation among points in S is defined, which considers equivalent all points sampled from the same curve $C_i(u)$, whenever the sampling conditions are anisotropic and constant over $\mathbb{R}^3$. For all $p, q \in S = \{p_0, p_1, p_2, ...p_n\} \subset \mathbb{R}^3$ one defines the *Extended Neighbor* relation $r()$ as:

$$r(p,q) \Longleftrightarrow (\exists [q_1, q_2, ..., q_w] \mid (q_i \in S) \\ \wedge (q_1 = p) \wedge (q_n = q) \wedge (|q_i - q_{i+1}| \leq \epsilon)) \quad (5)$$

Intuitively, a point p is in the extended neighborhood of a point q , if and only if there exists a sequence of points of the sample S between them, starting at p and ending at q such that no two points of the sequence are farther apart than a distance ϵ from each other.

The $r()$ relation defined above is an equivalence relation. It holds that:

$$r(P_i, P_i) \quad (6)$$
$$r(P_i, P_j) \wedge r(P_j, P_k) \rightarrow r(P_i, P_k)$$
$$r(P_i, P_j) \rightarrow r(P_j, P_i)$$

The properties of the relation $r()$, Extended Neighbor, in (6) allow to partition the set S into a number of subsets $S_1, S_2, ..., S_w$ such that $\cup_i S_i = S$ and $S_i \cap S_j = \phi, i \neq j$. Each S_i of the partition is the set of points sampled from the curve $C_i(u)$. The partition of the set S by using the equivalence relation $r()$ is realized by using an algorithm of *transitive closure*. For details about transitive closure algorithms or equivalence relations see (Suppes, 1972).

3. ALGORITHMS

Algorithms for determining a PL approximation for quasi-planar 1-manifolds in $\mathbb{R}^3$ are presented in this section, along with two figures that show partial results obtained at the main steps of each algorithm.

3.1. Data Pre-Processing

The point data must be pre-processed in this sequence: (i) Scaling: to guarantee that a standard bounding box of the S set is available, since both PCA and Least Squares estimation is sensitive to such aspects. (ii) Partition: to identify point subsets of S which are originated in the sample of disjoint $C_i(u)$ curves. (iii) Identification of Best Plane: to find a statistically plane $\amalg$ fit to the quasi-planar point set S. (iv) Correction to Planar Set: to project S onto Π in order to have a perfectly planar point set. (iv) Transformation of XY Plane: to use the algorithmic results in literature which deal with point sets in plane XY. Step (i) is required since cross cuts of branched shells lead to unconnected regions. A post-processing step consists in (v) the application of inverse transformations, in order to bring the found solution back to the original space.

3.2. Optimal Local Point Set Estimation

Given a point cloud in space π_i, result of a statistical sample with variance $[\sigma_x, \sigma_y, \sigma_z]$ from a 1-manifold $C_i(u)$ (possibly with border) in $\mathbb{R}^3$ one is interested in estimating the tangent line $dC_i(u)/du|_{u=u^*}$, at point $C_i(u^*)$ of the curve $C_i(u)$. PCA and Least Squares are applied on points of the sample which are contained inside a ball $B(P_s, R)$, centered at a seed point P_s with a radius R. Two competing aspects must be compromised: (i) a small enough neighborhood (R) in the data set S must be considered to fit a linear estimation of the local tangent. (ii) as the population of point samples decreases with R, the goodness of the linear estimation decreases as well. To achieve (i) and (ii) a search is conducted for a local optimal combination of P_s and R for the linear fitting of local neighborhoods of S.

The search basically starts with a ball $B(P_0, R_0)$ enclosing a set S_0 of points. Applying the PCA to the point set, a measurement of the fitting error is found. Lowering such an error by variating R_k within a fixed interval generates changing point sets, which have evolving centers of gravity P_k. With this ad hoc process it was found a good convergence to find a combination of P_k and R_k to produce a local minimum of the fitting error.

3.3. Principal Curve with PCA and Delone Triangulation

The following discussion will be illustrated using a planar 1-manifold with Border (open $C_i(u)$). Later on, the concepts explained will be applied on self-intersecting planar 1-manifolds.

For planar self-intersecting curves PCA alone is not robust enough. Additional processing is required since the points in the neighborhood of the intersection are exhausted for purposes of PCA estimation as the PL approximation crosses the first time over the intersection neighborhood. As the PL curve revisits the intersection neighborhoods no points are available for iden-

tifying the trend of curve, and the algorithm tends to look for another point (i.e. curve) neighborhood where to work, without really having reproduced the intersection. The result is an incomplete curve stage, therefore missing the self-intersection detail.

Because of this reason, it was decided to determine the minimal tape-shaped polygon T covering S, the point sample of $C_i(u)$. The minimal tape-shaped polygon for a point sample in $\mathbb{R}^2$ is the boundary of the minimal-area, connected 2D region, possibly with holes, and not necessarily convex, including all points in the set. This polygon will have holes for closed or self-intersecting $C_i(u)$. T will be carved from the Delone Triangulation $DT(S)$ of the point set S (see (Fortune, 1995) and (Guibas & Stolfi, 1985)). The extent of the carving to get a *minimal* T covering S is decreed by the PCA estimations run on the point set. Finally, an *approximation* of the medial axis of T, called here the *skeleton of* T, is the PL approximation of the $C_i(u)$ curve.

Figure 1(a) shows a data set from a planar non self-intersecting curve sampled with a stochastic process. The figure presents a data set which has been already resized, its best plane estimated, and their points projected onto this plane, which produces a coplanar subset. The Delone Triangulation of this point set is displayed in Figure 1(b).

Filtering of Delone Triangles

The minimal polygon T is found by eliminating triangles from the Delone Triangulation of the points set S. The Delone Triangles will be filtered out based on the following criteria: (a) Area, (b) Approximate enclosure in the PCA neighborhood (optimal ball), (c) Edge Length, (d) Vertex perpendicular departure from local tangent lines to $C_i(u)$ and (e) Aspect Ratio. However, in order to apply such methods, "reasonable values" of the area and edge length of Delone triangles belonging to the "tape" containing the point set need to be estimated. For such purpose a PCA is run iteratively on neighborhoods of the data set, thus determining the line $\vec{L}(\eta) = \vec{P_v} + \eta * v$ that best approaches the tangent to the $C_i(u)$ curve in that neighborhood. Delone triangles contained within a scaled version of this ball, namely $f_D * B(P_v, R_o)$ (with $f_D = 1.3$ an enlarging factor) might be considered as "typical" of the ones forming the T, and therefore rendering "typical area" $\bar{A}$ and "typical edge length" $\bar{l}$ values. The criteria to classify a Delone triangle as belonging (or not belonging) to the tape are:

1. **Enclosure**: Accept a Delone triangle DT_i if it is contained within the local PCA ball, that is, if $DT_i \subseteq B(P_v, R_o)$ where $B(P_v, R_o)$ is the best local PCA ball (see Figure 1(c)).

2. **Area and Edge Length**: Reject a Delone triangle DT_i if its Area or maximum Edge Length are too large. That is, if $(Area(DT_i) \geq f_A * \bar{A})$ or if $(E_{max} \geq f_l * \bar{l})$ respectively, for constants f_A and f_l. Figure 1(d) shows Delone Triangles surviving this criterion.

Polygon Synthesis based on Filtered Delone Triangulation

Polygon after application of criteria 1 and 2 is shown in Figure 1(d). The triangles surviving the area criterion are dark colored, while the ones surviving the edge length criterion are light colored. Each edge of a Delone triangle DT has 1 or 2 triangles which are incident to it, with the following characteristics:

1. Edges $e_{i,j}$ in which Delone triangles DT_i and DT_j are incident are not internal to the tape-shaped 2D region.

2. Edges e_i in which only one Delone triangle DT_i is incident are the boundary ∂T of the tape-shaped 2D region T. They may be either in the outermost loop, or in the internal loop.

The classification of internal vs external edges in a 2-manifold with boundary (Fomenko & Kunii, 1997), (Morse, 1934) is characteristic of Boundary Representations. Additional information on Boundary Representation may be found in (Mantyla, 1988).

Medial Axis VS. Principal Curve

Figure 1(d) presents the T minimal polygonal region that covers the point set S. The boundary ∂T of the 2D band-shaped polygon T, built by filtering the original Delone Triangulation, is colored black in Figure 1(e). Care must be exercised, however, because such a figure shows a new Delone Triangulation (for the point resample of the boundary ∂T). Therefore, the point set for this second Delone Triangulation is not the original S-shaped point set.

An approximation to the *medial axis* $MA(T)$ of T is a skeleton $SK(T)$, which is built in this manner (Geiger, 1993), (Boissonnat, 1988):

1. Construct the Voronoi Diagram $VD(T)$ and Delone Triangulation $DT(T)$ of the vertices of T (see Figure1(e)).

2. Keep from $DT(T)$ only the Delone triangles contained in T. Call this set $\overline{DT(T)}$.

3. Keep from $VD(T)$ only the Voronoi edges which are finite and are dual to the edges in $\overline{DT(T)}$. Call this set $\overline{VD(T)}$.

4. If $\overline{VD(T)} \not\subseteq T$ then re-sample ∂T with a smaller interval and go to step 1 above. Otherwise, $\overline{VD(T)}$ is the sought skeleton of T, $SK(T)$.

As evident from Figure 1(f), a PL approximation of the 1-manifold $C_i(u)$ is the skeleton axis of $SK(T)$ the polygonal region T.

Notice that several resamples of ∂T may be needed to converge to $SK(T)$. Figure 1(e) shows one of such resamples. The boundary ∂T of the S-shaped polygon T in Figure 1(f) is sampled with a small enough interval. This tight sampling guarantees that the portion of the Voronoi Diagram confined to T, $SK(T)$, is acceptable as an approximation of $MA(T)$, the medial axis of T.

Figure 4 presents a comparison of the two skeletons: (a) the interrupted one is achieved by direct application of PCA. (b) the continuous skeleton is found by filtering of the Voronoi Diagram assisted by PCA as per the process in Figure 1.

3.4. Curve Reconstruction with Least Squares

After the data pre-processing steps mentioned in Section 3.1, the Least-Squares-based algorithm takes as input a set S of quasi-coplanar points, and returns a polyline that fits these points by performing the steps listed below.

Radius Variation

An initial ball $B_0\,(p_0, r_0)$ and the set P_{B0} composed by the points in S that lie inside of it i.e. $P_{B0} = \{p \in S : p \in B_0\}$ is defined. Since p_0 is a point randomly selected from S, the polyline reconstructed from a same point set may vary at each run. The magnitude of the radius and the coordinates of the center of B_k, are then repeatedly varied so that the fitting error of a least square regression calculated for P_{Bk} is minimized. Let $\epsilon\,(p, r)$ be a function that associates a least-square regression fitting error to the points inside a ball with center p and radius r. It is desired to find the values of p and r that minimize ϵ. We first proposed an algorithm that calculated ϵ for several values of r and several values of p, and returned the pair of values that minimized ϵ among the values analyzed. The following variation of this algorithm was used for this case. The radius of the ball is varied from an upper bound r_u to a lower bound r_l, using a step dr. Let R denote the set of possible radius for each ball:

$$R = \{r_u, r_u - 1dr, r_u - 2dr, \ldots, r_u - i \cdot dr, \ldots, r_l\}$$

Now, let B_{k_i} and $B_{k_{i+1}}$ be two consecutive possible balls. In order to also vary the center of the ball in each iteration, the centroid of the points contained in B_{k_i} is calculated, and it will be used as the center for the ball $B_{k_{i+1}}$.

Polyline Reconstruction

The centroid of the points contained in the ball for which the fitting error was minimized in the previous step, is added to the ordered set of vertices of the recovered polyline. For each $r \in R$ the slope m_{k_i} of the correspondent least-square regression is calculated. The error between a line with slope m_{k_i} pivoted in the center of the ball B_{k_i}, and the points in B_{k_i} is calculated. The ball B_{k*} for which the error was the lowest among all analyzed balls is selected as the best ball. The centroid of the points in S that lie inside B_{k*} is calculated, and added to the recovered polyline.

Then, an initial center for B_{k+1} is determined. For this purpose m_{k*} is vectorized i.e. a vector

$$V_{k*} = \langle 1, m_{k*}, 0 \rangle$$

is associated to m_{k*}. Since two vectors with opposite directions can be associated to m_{k*}, a comparison between the vector associated to m_{k-1*} and V_{k*} is made, by calculating the angle between them. If the value of this angle is not within $-\pi/2$ and $\pi/2$, then

$$V_{k*} = \langle -1, -m_{k*}, 0 \rangle$$

Let $B_{k+1}\,(p_{k+1}, r_{k+1})$ denote the new ball whose center is to be calculated. p_{k+1} is obtained by moving along V_{k*} a certain distance. In this case

$$p_{k+1} = p_{k*} + \lambda r_{k*} \cdot V_{k*}$$

where p_{k*} and r_{k*} are respectively the center and radius of B_{k*}, and λ is an advance ratio. An adequate value for λ was calculated after applying the algorithm

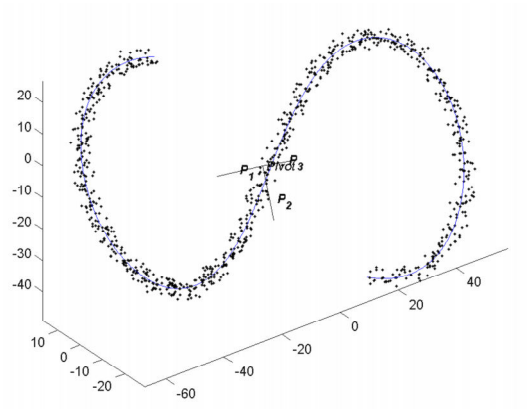

(a) Point Sample of Planar S-shaped $C_i(u)$ Manifold.

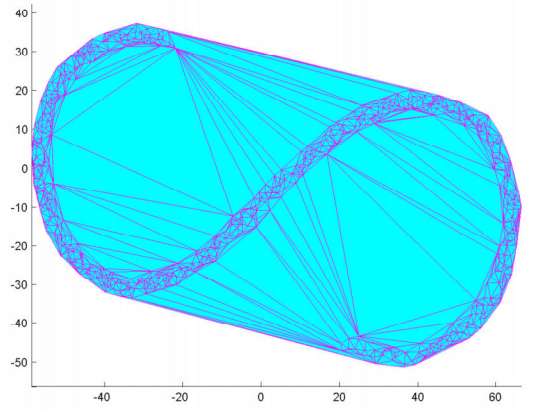

(b) Delone Triangulation of S-shaped Planar Point Sample.

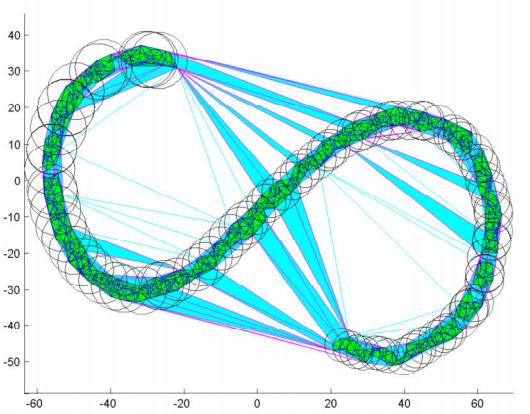

(c) Filtering of Delone Triangulation with PCA Balls.

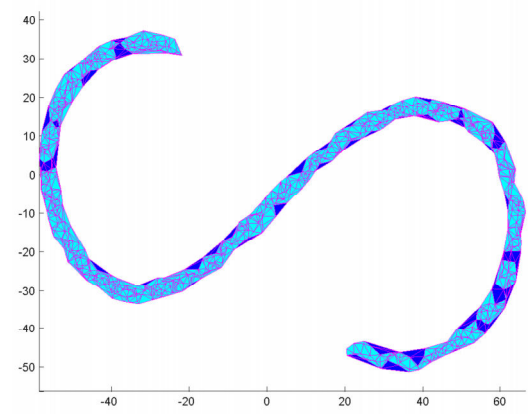

(d) Selected Triangles by Area and Length Criteria.

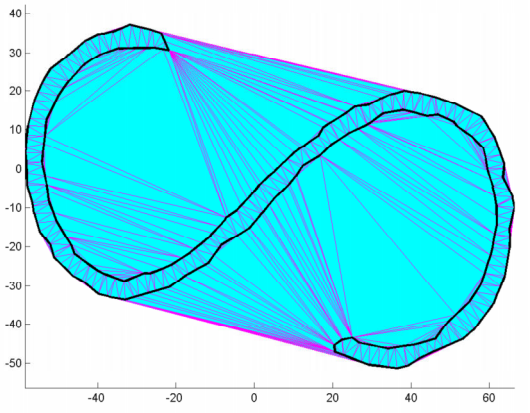

(e) Band Polygon and its Delone Triangulation

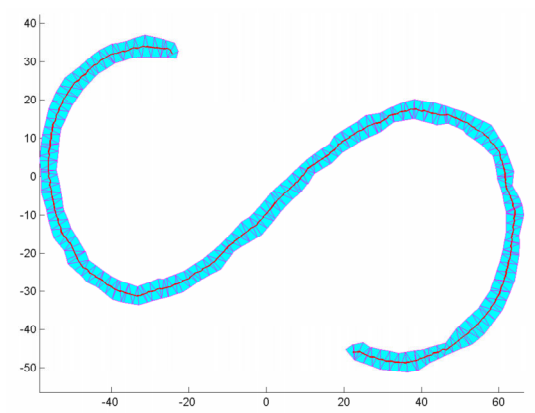

(f) Filtered DT and Skeleton

Figure 1 Piecewise Linear Approximation of S-shaped $C_i(u)$ by Combined PCA and Voronoi-Delone Methods

to several different sets of points.

The steps mentioned above are iterated for each of the S_i, until all points in S have been covered by at least one ball (see Figure 2(b)). Figure 2(c) shows the curve reconstructed from the point cloud (see Figure 2(a)) obtained from a Range Images Multi-Mesh sample.

4. RESULTS

Section 4.1 illustrates the results of the PCA and Delone Triangulations methodology in dealing with the PL Approximation of planar 1-manifolds without Border (closed $C_i(u)$). Section 4.2 illustrates three curve reconstructions obtained for open, non-smooth, self-intersecting, and non-uniform sets, using the Least-Squares-based process.

4.1. PCA and Delone Triangulations Results

As before, the point sample of $C_i(u)$ renders a quasi-planar point set. According to the discussion, an isotropic scaling was applied to the point set, because PCA is sensitive to dimensional issues. PCA was then applied to estimate the best plane Π fit to the point set, and the modified Householder transformation was used to project all points onto Π. In addition, a rigid transformation is used to bring the (now perfectly) planar point set on the plane XY, where the process described in section 3.1 is followed. Figure 3(a) shows the initial point set, along with a coordinate frame attached to the plane Π. The Delone Triangulation of the point set projected onto Π is illustrated in the Figure 3(b). An intermediate stage of the acceptance of triangles included in the PCA balls is shown in the Figure 3(c). This is a very conservative criterion and therefore Delone triangles rejected in this part are not so in definitive manner. They may still be included if the Edge Length or Area criteria determine that they are part of the T tape-shaped polygon covering the point cloud path (see Figure 3(d)). After the region T has been synthesized by clustering Delone triangles chosen according to the PCA, Edge Length, and Area criteria, the boundary ∂T of the 2-manifold T, must be determined. This step is a standard procedure in Boundary Representation construction and is conducted according to rules in section 3.3. Out next goal is to identify the Medial Axis (MA) for polygon T. An exact calculation is out of question because MA results in curved portions. However, if a resample RT of T is fine enough, its medial axis may be approximated as the sequence of Voronoi Edges of RT, completely included in T. The *border* ∂T is resampled (see Figure 3(e)) and a new Delone Triangulation calculated and purged for this new point set. The purged Delone Triangulation is intended to keep only the Delone Triangles which cover or include the point cloud. Triangles from the Delone Triangulation which complete the convex hull of the point set but do not include points of it are eliminated. In this form, again, the T polygon is re-triangulated, but this time with triangles whose circumscribed center lies inside T. The loci of such centers is $SK(T)$, the skeleton approximation for $MA(T)$, the medial axis of T (see Figure 3(f)).

As seen in Figure 3(f), it is possible that the re-triangulation of T breaks this region into separate ones. This result is expected, since it indicates the presence of self-intersections in the original set, and corrects them by splitting the tape polygon T into annulus sub-parts T_i. Care must be still exercised, as $SK(T)$ may be outside of a T_i region, as shown in Figure 3(f). This situation, however, is not harmful since the skeletons SK_i do not intersect each other, and therefore serve as PL approximations for the original $C_i(u)$ curves.

Figures 4(a) and 4(b) show in red the PL approximation by using combined Voronoi-Delone methods plus PCA. Interrupted segments originate in the usage of PCA alone. Both Figures correspond to different point sets scaled in the Y direction, therefore rendering different PL approximations. In both examples, (i) the combined algorithm has superior performance, and (ii) the continuous skeleton approximates very closely the original curve $C_i(u)$.

4.2. Least Squares Fitting Results

The Least-Squares-based algorithm was tested on several unorganized and fuzzy point sets, which include non-uniform, non-smooth, near self-intersecting, and self-intersecting ones. Figure 5 presents the results obtained for three of these sets. Near self-intersecting, non-uniform point clouds, as the one shown in Figure 5(a), can be adequately reconstructed by varying the length of the segments of the reconstructed polyline, considering the dispersion of the sample of points contained in each ball. The radius variation process, described in section 3.4, results useful for this purpose. As mentioned in Section 3.3, a PCA (Least Squares in this case) algorithm alone is not robust enough for reconstructing self-intersecting point clouds. However, due to the randomness of the starting point of the reconstruction, mentioned in Section 3.4, certain runs

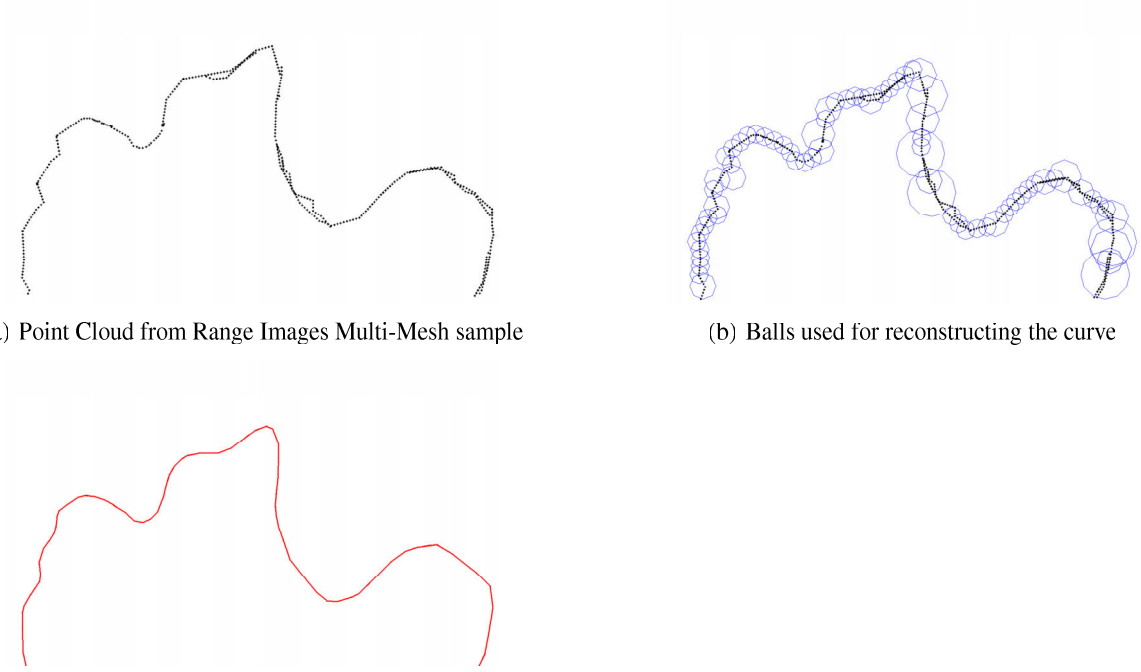

(a) Point Cloud from Range Images Multi-Mesh sample

(b) Balls used for reconstructing the curve

(c) Reconstructed Curve

Figure 2 Least-Squares-Fitting-based Reconstruction of Piecewise Linear 1-Manifold

can result in adequately-reconstructed self-intersecting point clouds (see Figure 5(c)).

In order to reconstruct point clouds with non-smooth sections (see Figure 5(b)), additional tools that consider the angles between the segments of the reconstructed polyline were included in the algorithm. Weighted Least Squares method was initially considered also for this purpose, but was temporally discarded since weighting criteria were not carefully determined. Notice also that criteria for identifying the endings of *open* point clouds are needed in order to *correctly* reconstruct open curves. A point-cloud-ending identification criterion based on the length of the reconstructed polyline segments, was included in our algorithm.

5. SURFACE RECONSTRUCTION FROM RANGE IMAGES

Range imaging is a technique for digitizing three-dimensional objects, given a set of range pictures. A range picture is a function $[I \times J] \to \mathbb{R}^3, \langle i, j\rangle \mapsto P_{ij}$, where $[I \times J]$ is the grid of pixels in the range picture, and $P_{ij} = \langle x_{ij}, y_{ij}, z_{ij}\rangle$ is the point in the surface of the optically sampled object, captured by the pixel in position ij of the grid of pixels.

It might be the case that no single range pictures suffices to describe the entire object, which makes necessary combining a collection of range images (see Figs. 6(a) and 6(b)) into a single triangular mesh that completely describes the object. The steps listed below were followed in order to generate such mesh: (i) Determining an initial alignment of the meshes with each other; (ii) Building a sample of points on the meshes; (iii) Using the algorithm discussed in Section 3.4 to reconstruct a set of curves (contours) from the sampled points; and (iv) Linking the recovered contours to generate the resulting mesh. In order to illustrate the mesh integration process, we present the results obtained when reconstructing Aphrodite's sculpture head. The Range Images data are courtesy from Fraunhofer Institute Computer Graphics, Darmstadt, Germany.

In step (ii), a set of K parallel planes are defined, and the intersection between each plane and the collection of shells recovered from the range images is calculated. A set of coplanar samples of points $S_1, S_2, \ldots, S_k, \ldots, S_K$ is generated by sampling the polylines resulting from each intersection. Figure 2(a) shows one of such coplanar samples $S_k = \{P_{0_k}, P_{1_k}, \ldots, P_{N-1_k}, P_{N_k}\}$ for Aphrodite's head model.

More than 100 levels (the number and separation dictated by the Nyquist criterion applied in the axial direc-

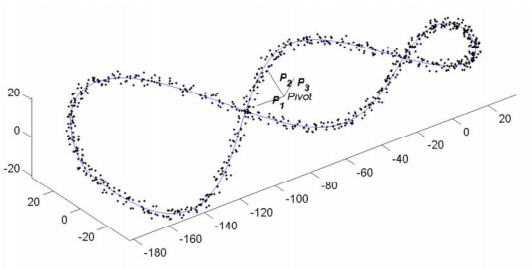

(a) Point Sample of Planar Double-8 $C_i(u)$ Manifold.

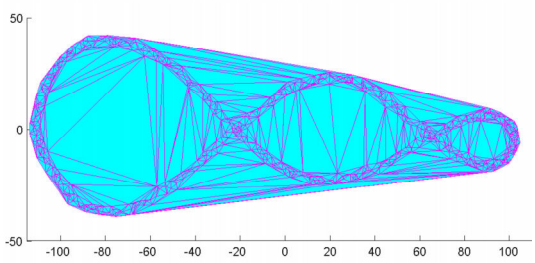

(b) Delone Triangulation of Planar Double-8 Point Sample.

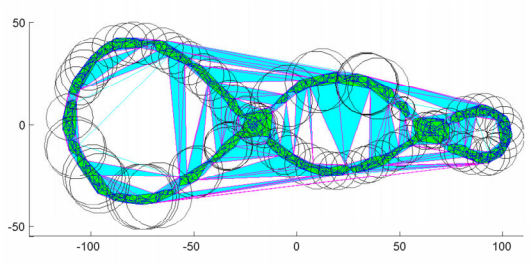

(c) Filtering of Delone Triangulation with PCA Balls

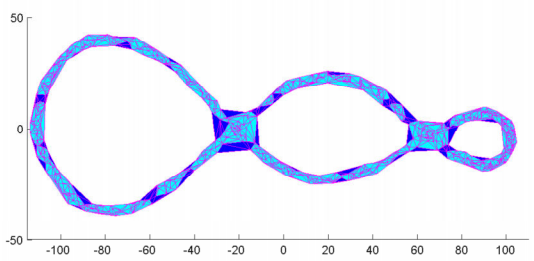

(d) Selected Triangles by Area and Length Criteria.

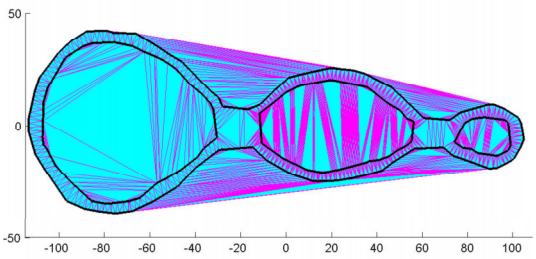

(e) Band Polygon and its Delone Triangulation

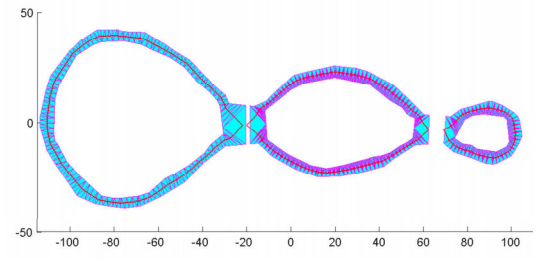

(f) Filtered DT and Skeleton

Figure 3 Process of PL Approximation of Double-8 self-intersecting $C_i(u)$ by Combined PCA and Voronoi-Delone Methods

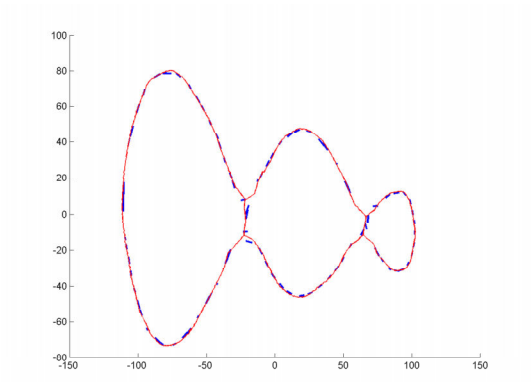

(a) Result Alternative 1: Multi-Polygon Result. Comparison PCA (blue) and VD+PCA (red) Results

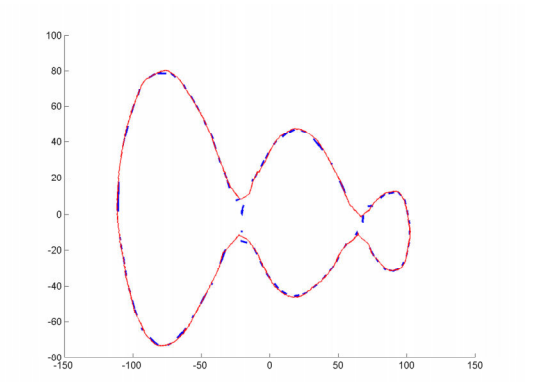

(b) Result Alternative 2: Single Polygon Result. Comparison PCA (blue) and VD+PCA (red) Results

Figure 4 Final Results. PL Approximations of Double-8 self-intersecting $C_i(u)$ by Combined PCA and Voronoi-Delone Methods

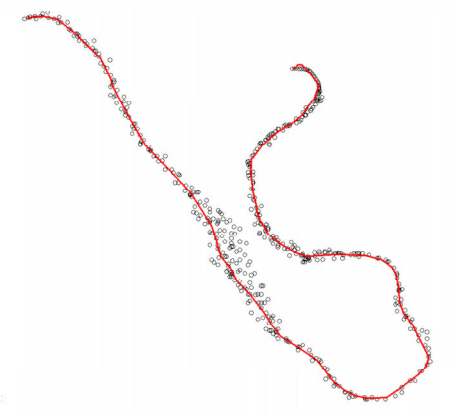

(a) Near Self Intersecting, Non-Uniform Point Cloud

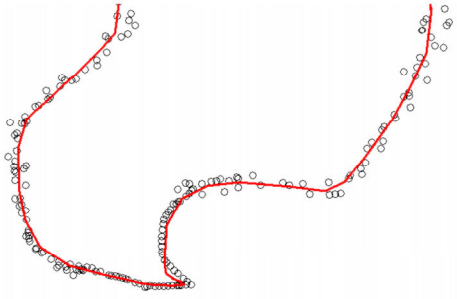

(b) Non-Smooth Non-Uniform Point Cloud

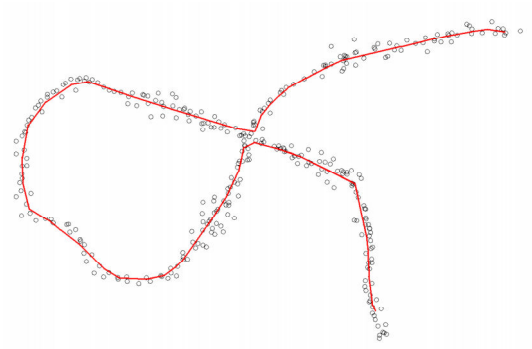

(c) Self Intersecting Non-Uniform Point Cloud

Figure 5 Curve reconstructions obtained for three different point sets by Least-Squares-based process.

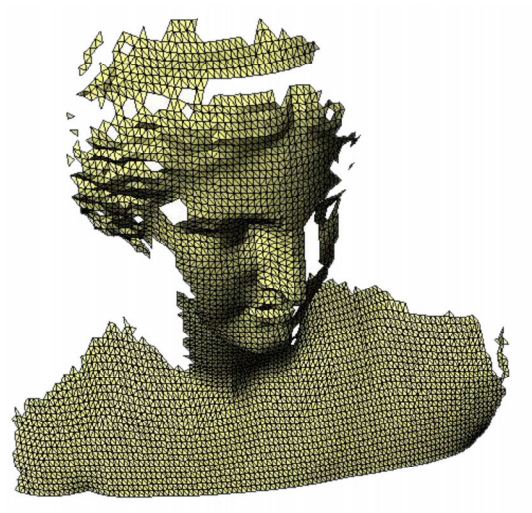

(a) $i-th$ Mesh from Front Range Image i Aphrodite

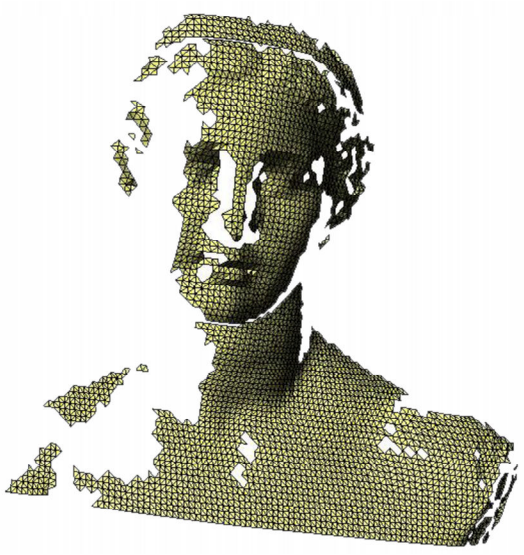

(b) $k-th$ Mesh from Front Range Image k Aphrodite

Figure 6 Range Image Data Set. Courtesy from Fraunhofer Inst. Computer Graphics, Darmstadt, Germany

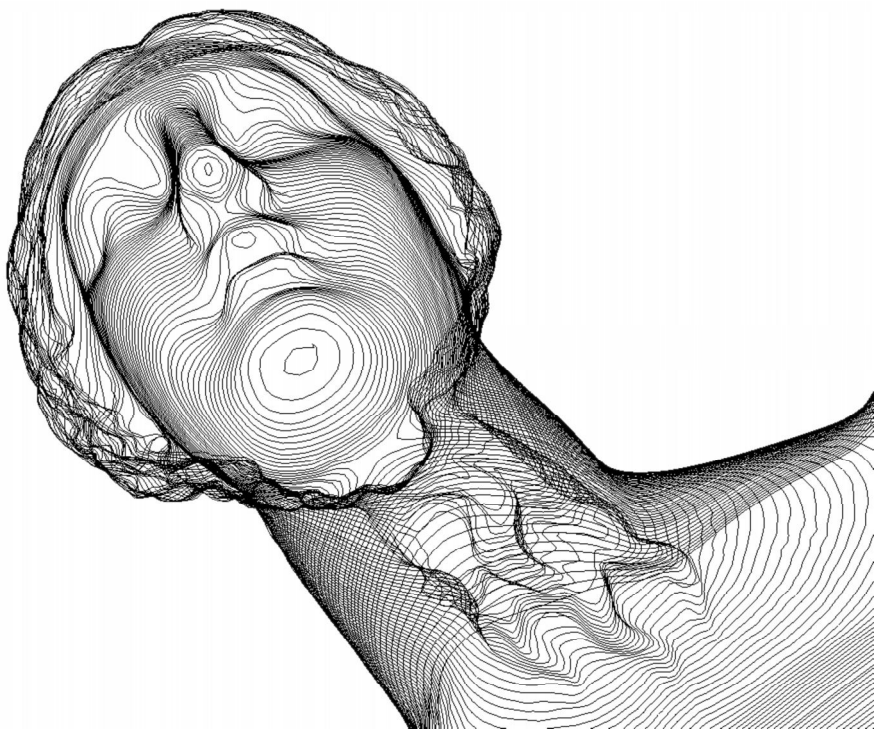

Figure 7 Aphrodite's head contours recovered from coplanar samples of points. Test data courtesy from Fraunhofer Inst. Computer Graphics, Darmstadt, Germany

tion) of coplanar points were obtained from sampling the collection of meshes corresponding to Aphrodite's sculpture head and neck, and same number of polylines were reconstructed from these sets (Figure 7). In spite of the large number of range pictures available for Aphrodite's sculpture, some of its regions were not covered by any of these, and therefore several sets of points needed to be manually completed. Once the sets were completed, none of the reconstructed polylines were edited. The surface reconstructed from the integrated, stochastically recovered contours is shown in Figures 8(a) to 8(c). Figures 8(a) and 8(b) correspond to resampling planes which are not orthogonal, and to an unfinished reconstruction (there is still a border). Figure 8(c) represents the integrated result for XY digitization planes. The final Aphrodite's surface reconstruction, composed by more than 65 000 triangular faces, is shown in figure 8(d).

6. CONCLUSIONS AND FUTURE WORK

Two methods, combining statistical and deterministic techniques, for reconstructing PL 1-manifolds from unorganized coplanar, fuzzy point sets have been discussed. The first method (PCA-assisted Voronoi-Delone) reaches the point of synthesis of the $SK(T)$ skeleton of the tape-shaped 2D region covering the point set S. This skeleton is a planar graph, but is not necessarily a 1-manifold, as it has branchings. The elimination of the branches is needed, but represents no significant demeanor in the presented results, as existing algorithms for graph splitting are applicable.

The second method (Least-Squares fitting march along the point cloud) is useful for cases when calculating eigenvalues and eigenvectors is not possible. This method returned correct reconstructed PL 1-manifolds for non-trivial point sets (open, unorganized, fuzzy, non-uniform, non-smooth, near self-intersecting). A Least Squares assisted Voronoi-Delone method is desired for reconstructing self-intersecting point sets. Additional criteria to obtain a more robust reconstruction algorithm for point sets with non-smooth sections could be provided by using Weighted-Least-Squares technique.

An application of the second method to surface reconstruction from Range Imaging was also discussed, and results for a real model were presented. Our integration method correctly joined together a set of

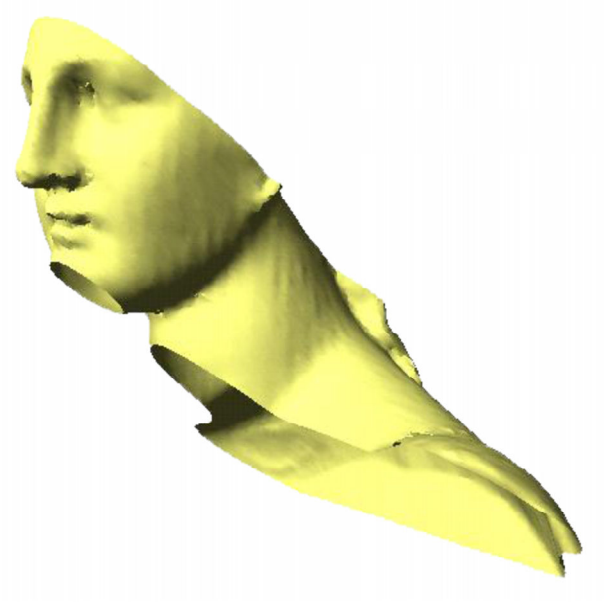

(a) Integrated Aphrodite with border. Smooth Render

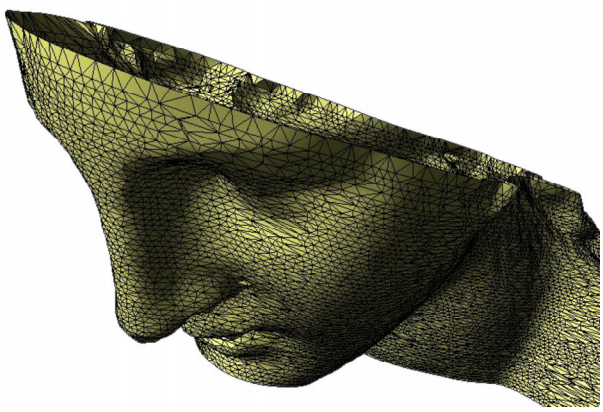

(b) Integrated Aphrodite with border. Wireframe

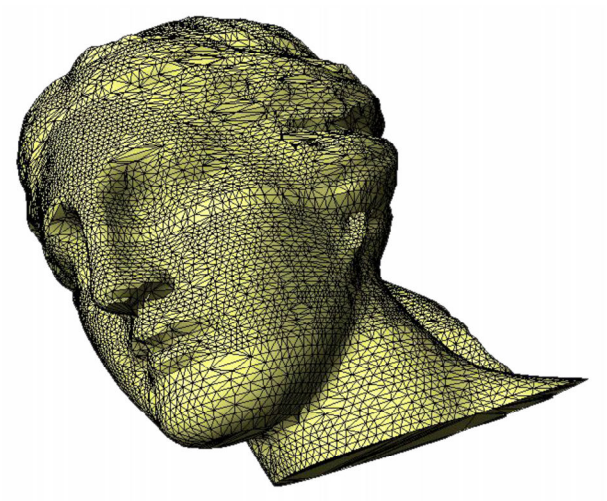

(c) Integrated Aphrodite without Border. Wireframe

(d) Integrated Aphrodite without Border. Smooth Render

Figure 8 Results of Range Picture Integration. Test data courtesy from Fraunhofer Inst. Computer Graphics, Darmstadt, Germany

meshes obtained from several Aphrodite's sculpture head Range Images, into a 65 000-triangles model.

REFERENCES

Althaus, E. & Mehlhorn, K. (2000). Polynomial time TSP-based curve reconstruction. In Symposium on Discrete Algorithms (SODA), pp. 686–695.

Althaus, E., Mehlhorn, K., Näher, S., & Schirra, S. (2000). Experiments on Curve Reconstruction. In ALENEX, pp. 103–114.

Boissonnat, J. (1988). Shape reconstruction from planar cross-sections. Computer Vision, Graphics and Image Processing, 44, pp. 1–29.

Edelsbrunner, H. (1998). Shape reconstruction with the Delaunay complex. In LATIN'98: Theoretical Informatics, volume 1380 of Lecture Notes in Computer Science, pp. 119–132.

Edelsbrunner, H. & Mücke, E. (1994). Three-dimensional alpha shapes. ACM Transaction on Graphics, 13, pp. 43–72.

Fang, L. & Gossard, D. (1992). Fitting 3D curves to unorganized data points using deformable curves. In: Visual Computing, Proceedings of CG International, pp. 535–543.

Fomenko, A. & Kunii, T. (1997). Topological Modeling for Visualization. Tokio: Springer Verlag.

Fortune, S. (1995). Voronoi Diagrams and Delaunay Triangulations. In Computing in Euclidean Geometry, Lecture Notes Series on Computing 4, World Scientific, pp. 225–262.

Geiger, B. (1993). Three dimensional modeling of human organs and its application to diagnosis and surgical planning. In Research Report 2105, INRIA, Sophia-Antipolis, Valbonne, France.

Guibas, L. & Stolfi, J. (1985). Primitives for the manipulation of general subdivisions and the computation of voronoi diagrams. ACM Transactions on Graphics, 2(4), pp. 74–123.

Lee, I. (2000). Curve reconstruction from unorganized points. Computer Aided Geometric Design, 17(2), pp. 161–177.

Mantyla, M. (1988). An Introduction to Solid Modeling. Maryland, USA: Computer Science Press.

Morse, M. (1934). The calculus of variations in the large. New York: American Mathematical Society.

Suppes, P. (1972). Axiomatic Set Theory. New York: Dover Publishing.

T, T. H. & Stuetzle, W. (1989). Principal curves. Journal of the American Statistical Association, 84, pp. 502–516.

Taubin, G. & Ronfard, R. (1996). Implicit simplicial models for adaptive curve reconstruction. IEEE Transactions on Pattern Analysis and Machine Intelligence, 18(3), pp. 321–325.

Turk, G. & Levoy, M. (1994). Zippered Polygon Meshes from Range Images. In SIGGRAPH'94: Computer Graphics Proceedings, Annual Conference Series, pp. 311–318.

Verbeek, J., Vlassis, N., & Kröse, B. (2001). A soft k-segments algorithm for finding principal curves. Proc. Int. Conf. on Artificial Neural Networks, pp. 450–456.